

C 2

NACA RM E54L06



RESEARCH MEMORANDUM

PRESSURE-DROP CHARACTERISTICS OF A 22-SEGMENT
 MOCK-UP OF THE GENERAL ELECTRIC COMPANY
 AIR-COOLED AIRCRAFT REACTOR

By Eldon W. Sams and Walter F. Weiland, Jr.

Lewis Flight Propulsion Laboratory
 Cleveland, Ohio

RECEIVED
 JAN 21 1955
 NATIONAL ADVISORY COMMITTEE
 FOR AERONAUTICS
 WASHINGTON, D. C.

NATIONAL ADVISORY COMMITTEE
 FOR AERONAUTICS
 WASHINGTON

January 20, 1955
 Declassified January 12, 1961

NATIONAL ADVISORY COMMITTEE FOR AERONAUTICS

RESEARCH MEMORANDUM

PRESSURE-DROP CHARACTERISTICS OF A 22-SEGMENT

MOCK-UP OF THE GENERAL ELECTRIC COMPANY

AIR-COOLED AIRCRAFT REACTOR

By Eldon W. Sams and Walter F. Weiland, Jr.

SUMMARY

An investigation was conducted to obtain pressure-drop data for flow of air with no heat addition on a 22-segment mock-up of the General Electric Company aircraft reactor. Pressure-drop data were obtained over a range of Reynolds numbers from about 10,000 to 100,000, Mach numbers up to about 0.40, and inlet-air pressures up to about 70 inches of mercury absolute. The results indicate that individual segment friction factors based on measured static-pressure drops corrected for non-friction losses fall about 65 percent above the Kármán-Nikuradse line for fully developed turbulent flow in smooth pipes. When segment length-to-effective-diameter-ratio effects are taken into account, however, the experimental data with exception of the first and last segments are in good agreement with results predicted by analysis.

INTRODUCTION

The General Electric air-cooled concentric-ring-type aircraft reactor appears as a right circular cylinder approximately 5 feet in diameter and 3 feet long through which cooling air flows axially. In the axial direction, the reactor fuel element core consists of a number of segments resulting from interruptions of the core surfaces at regular intervals. In a current design, 22 segments are being considered wherein each segment is 1.5 inches long with an interruption or gap of 0.125 inch between segments. In the radial direction, the reactor segments consist of a series of thin concentric plates having sinusoidal crimps (running

axially along the plates) at intervals around the circumference; the plates are separated by spacer strips between plates at the leading and trailing edges. Cooling air flows axially through the reactor segment passages and into the 0.125-inch gap between segments before entering the next segment. The equivalent diameter of the passages is varied from segment to segment by varying the distance between plates. The plate material consists of a stainless-steel-clad uranium oxide core having a total thickness of about 0.012 inch.

The present investigation was conducted to determine pressure-drop characteristics of the reactor. Accordingly, mock-ups of a small portion of each of the 22 fuel-element segments (representing a small frontal cross section through the entire length of fuel-element core) were tested at the NACA Lewis laboratory.

The tests were conducted over a range of Reynolds numbers from about 10,000 to 100,000, inlet-air pressures up to about 70 inches of mercury absolute, and Mach numbers up to about 0.40. The results are presented herein as curves of friction factor, against Reynolds number for all segments over the range of conditions investigated.

APPARATUS

Reactor segments. - The 22 reactor mock-up segments used in this investigation are shown in figures 1(a) and (b) and are numbered according to location in the air-flow path. The individual segments (each 2 by 3 by 1.5 in.) were constructed of 0.012-inch stainless steel with all joints welded. The 22 segments were alined in proper flow sequence with 0.125-inch gaps between segments; two 0.012-inch stainless-steel plates running the total length of segments were soldered to the individual segments, giving a continuous surface along the top and bottom sides of the assembly. The segments, assembled in this manner, are shown in figure 1(c); the segment assembly was supplied by the General Electric Company for the tests reported herein.

The geometric characteristics of the individual mock-up segments are given in table I.

Test setup. - A schematic diagram of the test setup used herein is shown in figure 2. As indicated in figure 2(a), supply air passed through a filter and pressure-regulating valve, an ASME-type flat-plate-orifice run with air straightener, and an inlet-air tank before entering the test section (tunnel containing mock-up segment assembly). A thermocouple located near the inlet tank measured the orifice and test-section inlet-air temperature. Air leaving the test section was rejected to the atmosphere through a valve used to establish the desired tunnel pressure.

A schematic diagram of the test section is shown in figure 2(b). The mock-up segment assembly (fig. 1(c)) was placed in a rectangular steel tunnel provided with a rounded entrance. Static-pressure taps were placed axially along the center line of the tunnel side wall, taps being located in the center of each 0.0125-inch gap between segments with additional taps upstream of segment 1 and downstream of segment 22. Taps were similarly placed along the opposite tunnel side wall (not shown) differing only in that each tap was offset from the center line sufficiently to fall between plates of the preceding segment. The pressure taps in either row were accurately located by placing a Lucite strip against the exposed side of the segment assembly (fig. 1(c)) for marking and drilling the desired tap locations in the Lucite, which in turn was used as a template for drilling the tunnel side walls for pressure taps. Static-pressure drops across the individual segments were read differentially on a series of U-tube water manometers; the taps were connected in such a manner as to allow each row of taps to be read independently of the other. Over-all pressure-drop readings were also obtained as a check on individual readings. A photograph of the test setup is shown in figure 3.

SYMBOLS

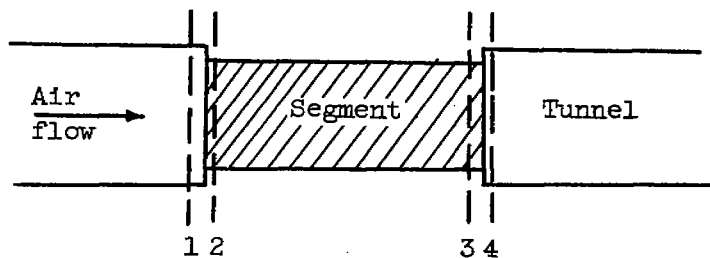
The following symbols are used in this report:

| | |
|----------------|---|
| A | free-flow area of segment, sq ft |
| D_e | effective diameter (reactor segment), $4A/P$, ft |
| F | free-flow factor (free-flow area/total frontal area) |
| $f/2$ | half-friction factor based on measured static-pressure drop |
| $(f/2)_{cor}$ | half-friction factor based on measured pressure drop corrected for nonfriction losses |
| $(f/2)'_{cor}$ | half-friction factor based on measured pressure drop corrected for nonfriction losses and L/D_e effects |
| G | mass velocity, (W/A) , lb/(sec)(sq ft) |
| g | acceleration due to gravity, 32.2 ft/sec ² |
| K_c | vena-contracta pressure-loss coefficient |
| L | length of reactor segment, ft |
| P | wetted perimeter of reactor segment, ft |

| | |
|-----------------|---|
| p | static pressure, lb/sq ft |
| Δp | measured static-pressure drop across reactor segment, lb/sq ft |
| Δp_{en} | entrance pressure drop, lb/sq ft |
| Δp_{ex} | exit pressure drop, lb/sq ft |
| Δp_m | momentum pressure drop, lb/sq ft |
| Δp_{vc} | vena-contracta pressure drop, lb/sq ft |
| Re | Reynolds number |
| t | static temperature, $^{\circ}R$ |
| Δt | static-temperature difference between entrance and exit of test segment (taken as zero), $^{\circ}R$ |
| V | velocity, ft/sec |
| W | air flow, lb/sec |
| X | distance from entrance, ft |
| α | $\Delta p/p_1$ |
| β | $\Delta t/t_1$ |
| ρ | air density, lb/cu ft |

Subscripts:

The subscripts used herein are defined by the following diagrammatic sketch of the test segment:



av indicates average for segment

RESULTS AND DISCUSSION

Measured static-pressure gradients. - A typical static-pressure-gradient curve obtained herein for the 22 reactor segments is shown in figure 4. The static pressure at the exit tap of each segment is plotted, in inches of water below reference (test-section inlet) pressure, against segment number. Pressure readings at two additional taps downstream of segment 22 are also shown.

As previously indicated, a row of static-pressure taps was provided along either side wall of the tunnel; the taps in one row (taps B) were located along the center line, and in the other row (taps A) slightly offset so as not to fall directly behind a plate. Readings from both sets of taps are plotted in figure 4. Inasmuch as the readings are in agreement for some segments and in random disagreement for others, the pressure gradient may be represented equally as well by a faired line through the data. The measured over-all pressure drop across the 22 segments, also plotted in figure 4 for both sets of taps, is in good agreement with the sum of the individual drops, indicating small reading errors.

Friction factor based on measured static-pressure drop. - The half-friction factors obtained herein for the 22 reactor segments are shown in figure 5(a) where half-friction factor based on measured pressure drop is plotted against Reynolds number. The half-friction factor is defined by the equation:

$$\frac{f}{2} = \frac{\Delta p}{8 \frac{L}{D_e} \frac{G^2}{2g\rho_{av}}} \quad (1)$$

where Δp is here and hereinafter obtained from the faired pressure gradient line (fig. 4), and ρ was evaluated using the total temperature and the average of inlet and exit static pressure for the particular segment.

Included in figure 5(a), is the Kármán-Nikuradse line representing the relation between friction factor and Reynolds number given by

$$\frac{1}{\sqrt{8 \frac{f}{2}}} = 2 \log \left(\text{Re} \sqrt{8 \frac{f}{2}} \right) - 0.8 \quad (2)$$

The data fall considerably above the reference line (eq. (2)) inasmuch as nonfriction losses have not been considered. Except for the data of the first and last segments (1 and 22), the friction factors fall in a narrow band through which a mean line has been drawn. The deviation in data for segments 1 and 22 will be discussed later.

Friction factor based on corrected pressure drop. - The half-friction factors for the 22 segments are replotted in figure 5(b) using the same coordinates and reference lines as in figure 5(a). In this case, however, the half-friction factor is based on measured pressure drop corrected for nonfriction losses for the particular segment. The equations used in calculating these losses are the same as those used in reference 1 where, in a similar investigation, friction data were presented for 10 reactor segments having a different plate (core) configuration. These equations give the segment entrance loss as

$$(\Delta p)_{en} = \frac{G_2^2}{2g\rho_1} (1 - F^2) \quad (3)$$

The exit loss as

$$(\Delta p)_{ex} = \frac{G_1^2}{g\rho_1} \left(\frac{1 + \beta}{1 - \alpha} \right) \left(1 - \frac{1}{F} \right) \quad (4)$$

the momentum loss as

$$\Delta p_m = \frac{G_2^2}{g\rho_1} \left(\frac{\beta + \alpha}{1 - \alpha} \right) \quad (5)$$

and the vena-contracta loss as

$$(\Delta p)_{vc} = K_c \frac{G_2^2}{2g\rho_1} \quad (6)$$

where K_c is a function of free-flow factor F of the segment, values of which were obtained from reference 2.

Accordingly, the corrected half-friction factor $\left(\frac{f}{2}\right)_{cor}$ is given by equation (1) when Δp is diminished by the sum of these losses pertinent to the particular segment considered.

The pressure-gradient curves for all runs (fig. 4, for example) indicate that only about one half of the calculated exit recovery (given by eq. (4)) for segment 22 occurs between the segment trailing edge and exit tap, a distance of 1/8 inch. For all other segments where this distance is 1/16 inch (center of 1/8-in. gap), the recovery is considerably less, which also accounts for the fact that data for segment 22 fall below the rest (fig. 5(a)). Moreover, since the fluid only partially expands into the 1/8-inch gap between segments, the entrance loss is also somewhat less than that given by equation (3). Inasmuch as the full calculated entrance and exit losses are essentially

equal in magnitude for the data herein, the actual values of these two losses are considered to cancel out, and hence are neglected except for segment 1 where the full entrance loss is taken out. Since the fluid only partially expands into the 1/8-inch gap, the vena-contracta loss also is somewhat less than that given by equation (6) wherein K_c is based on segment free-flow area to full tunnel cross-section area ratio. Hence, the vena-contracta losses were also neglected except for segment 1. The momentum loss was taken out for all segments.

The data for the 22 segments corrected for nonfriction losses in this manner are shown in figure 5(b); the bulk of the data falls about 65 percent above the reference line. In comparing the data with that for fully developed turbulent flow (reference line), the effects of L/D_e must also be considered. These effects consist of (1) a momentum loss accompanying transition from flat (at entrance) to some degree of fully developed velocity profile (at exit); and (2) an increase in average friction factor resulting from high shear stresses in the entrance region. (This region of high stress may occur over a considerable portion of the segment length.) These factors are accounted for in reference 3 wherein curves of average and local friction factor are presented as functions of X/D_e and Reynolds number for flow between parallel flat plates with uniform velocity profile at entrance. The ratio of average to fully developed friction factor (from ref. 3) for L/D_e values of 4.0 and 8.0 when applied to the reference line (fig. 5(b)) result in the predicted lines (dashed) shown; the L/D_e values of 4.0 and 8.0 bracket the range of segment L/D_e 's investigated herein with the exception of segment 22, which has an L/D_e of 10.5.

With the exception of segments 1 and 22, the data of figure 5(b) are well bracketed by the predicted lines and, in general, show the proper characteristic with increase in L/D_e from segment to segment. Moreover, the data for segment 22 might well be in agreement with predicted values if the exit pressure recovery from segment 22 (in excess of that for other segments) could be taken into account. The excess recovery for segment 22 was attributed to the exit tap being 1/8 inch behind segment 22 (This distance is 1/16 in. for all other segments). The data for segment 1 is about 30 percent greater than predicted; this difference cannot be explained although it is probably caused by the segment being in proximity to the rounded entrance of the tunnel where, in other investigations, similar discrepancies have been noted.

Effect of Mach number. - Additional pressure-drop data were obtained over the same range of Reynolds number but at a lower Mach number level than that for the previous data. These data were obtained by keeping the mass-velocity ρV level constant while increasing the pressure (and density) level to the highest value that could be obtained

without encountering leakage from gasket seals at the tunnel side walls and ends; these gaskets were required to allow installation and close adjustment of tunnel walls to fit the segments. The maximum inlet pressure obtained was about 70 inches of mercury absolute, which resulted in lowering the exit Mach number (segment 22) from 0.40 to 0.17 at the highest flow rate.

These high-pressure (low Mach number) data are shown in figure 6 in comparison with the previous low-pressure data wherein the corrected friction factor is plotted against Reynolds number. The high- and low-pressure data are in substantial agreement for all segments, indicating small effect of Mach number for the range investigated.

Effect of reversing segments. - As a further check on the pressure-drop measurements and corrections, as well as geometry effects that may be involved, the entire segment assembly (fig. 1(c)) was turned end for end in the tunnel and additional data taken. The friction data obtained with the elements reversed is compared with that obtained in the original sequence in figure 7 for one flow rate. The identification numbers refer to the segments proper and not to tunnel-location sequence, although these are identical for the previous (nonreversed) tests. Figure 7 indicates that the reversed data are somewhat more random, which may result from geometry effects or equally as well from tap mislocations (taps may not fall exactly in gap centers with elements reversed); nevertheless, the reversed data are in substantial agreement with the previous (nonreversed) data.

Comparison of reactor segment data. - For comparison with the 10-segment data of a similar investigation (ref. 1) the data obtained herein are replotted in figure 8, wherein the L/D_e correction previously discussed is applied to the individual datum points, thus giving the equivalent fully developed values. Included in figure 8 are the data for the 22 segments in the original order, and the data for the 10 segments of reference 1 having triangular-shaped passages. With exception of a few segments (principally segment 1 of this investigation and segment 4 of ref. 1), the data fall within ± 20 percent of the Kármán reference line for turbulent flow in smooth passages.

SUMMARY OF RESULTS

The results of tests to obtain pressure-drop data for flow of air with no heat addition on a 22-segment mock-up of the General Electric Company air-cooled aircraft reactor are summarized as follows:

1. The friction factors based on measured static-pressure drops corrected for nonfriction losses fall about 65 percent above the Kármán-Nikuradse line for fully developed turbulent flow in smooth pipes. When

segment length-to-effective-diameter-ratio effects are taken into account, however, the experimental data with exception of the first and last segments are in good agreement with results predicted by analysis.

2. The friction data, obtained at two different pressure levels, indicate no appreciable effect of Mach number over the range investigated (Mach numbers up to 0.40).

3. With segment length-to-effective-diameter-ratio effects taken into account, the friction factors obtained herein for the 22 segments are in good agreement with those of a previous investigation for 10 segments having a different core configuration.

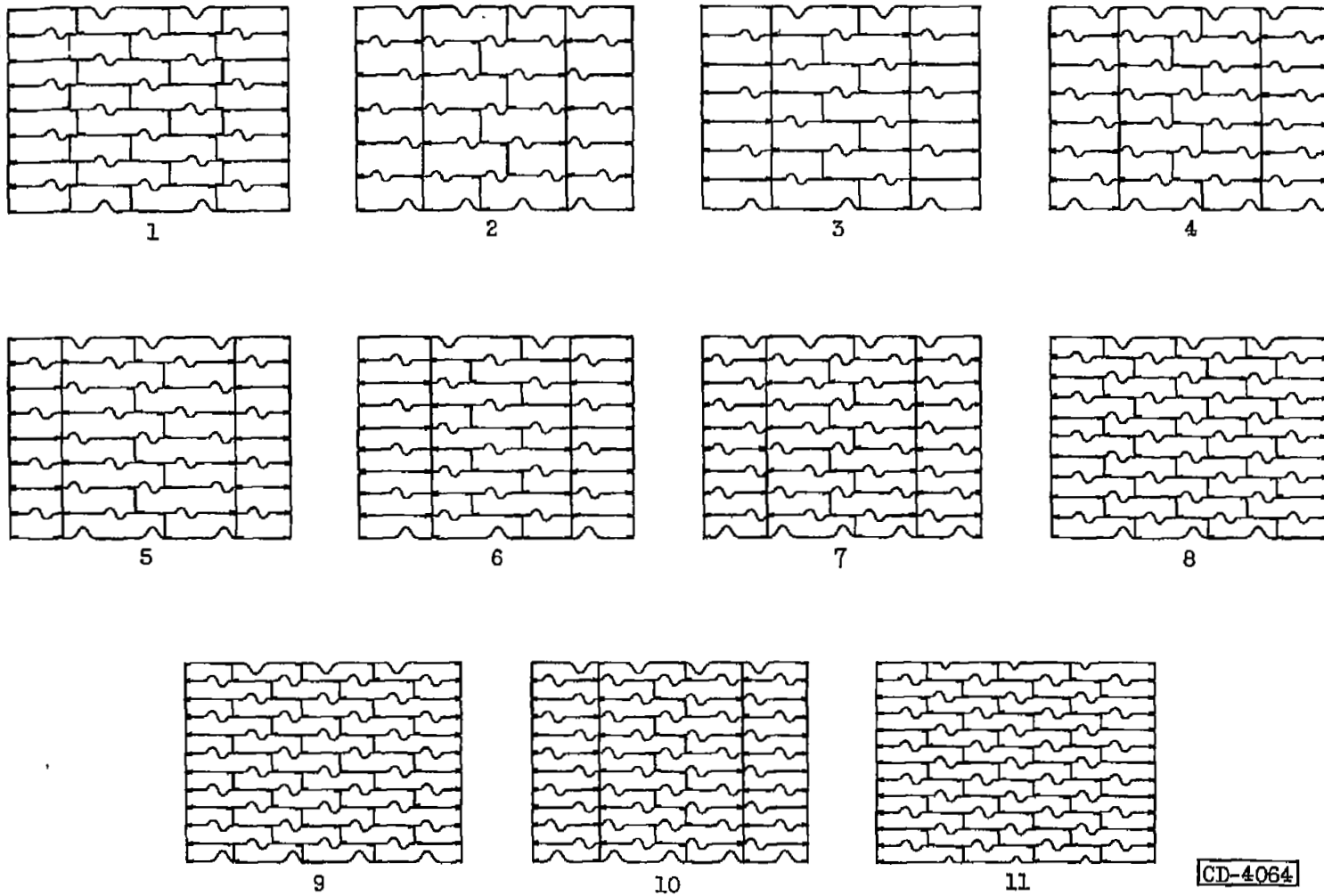
Lewis Flight Propulsion Laboratory
National Advisory Committee for Aeronautics
Cleveland, Ohio, December 6, 1954

REFERENCES

1. Sams, Eldon W., and Nagey, Tibor F.: Measurement of Friction Factors with no Heat Addition on Mockups of Ten Reactor Segments of the General Electric Company Air-Cooled Aircraft Reactor. NACA RM E53E01, 1953.
2. McAdams, William H.: Heat Transmission. Second Ed., McGraw-Hill Book Co., Inc., 1942, p. 122.
3. Deissler, Robert G.: Analysis of Turbulent Heat Transfer and Flow in the Entrance Regions of Smooth Passages. NACA TN 3016, 1953.

TABLE I. - GEOMETRIC CHARACTERISTICS OF SEGMENTS

| Reactor segment | Length, in. | Width, in. | Height, in. | Effective diameter, ft | Length-to-effective-diameter ratio | Free-flow area, sq ft |
|-----------------|-------------|------------|-------------|------------------------|------------------------------------|-----------------------|
| 1 | 1.50 | 3.00 | 2.00 | 0.0278 | 4.505 | 0.03802 |
| 2 | ↓ | ↓ | ↓ | .0335 | 3.731 | .03858 |
| 3 | ↓ | ↓ | ↓ | .0309 | 4.043 | .03834 |
| 4 | ↓ | ↓ | ↓ | .0296 | 4.225 | .03824 |
| 5 | ↓ | ↓ | ↓ | .0272 | 4.601 | .03797 |
| 6 | ↓ | ↓ | ↓ | .0251 | 4.983 | .03770 |
| 7 | ↓ | ↓ | ↓ | .0240 | 5.208 | .03757 |
| 8 | ↓ | ↓ | ↓ | .0223 | 5.597 | .03731 |
| 9 | ↓ | ↓ | ↓ | .0205 | 6.098 | .03697 |
| 10 | ↓ | ↓ | ↓ | .0200 | 6.250 | .03690 |
| 11 | ↓ | ↓ | ↓ | .0189 | 6.608 | .03665 |
| 12 | ↓ | ↓ | ↓ | .0181 | 6.912 | .03644 |
| 13 | ↓ | ↓ | ↓ | .0175 | 7.143 | .03633 |
| 14 | ↓ | ↓ | ↓ | .0167 | 7.463 | .03609 |
| 15 | ↓ | ↓ | ↓ | .0158 | 7.895 | .03588 |
| 16 | ↓ | ↓ | ↓ | .0157 | 7.979 | .03578 |
| 17 | ↓ | ↓ | ↓ | .0156 | 8.021 | .03577 |
| 18 | ↓ | ↓ | ↓ | .0152 | 8.242 | .03567 |
| 19 | ↓ | ↓ | ↓ | .0156 | 8.021 | .03577 |
| 20 | ↓ | ↓ | ↓ | .0156 | 8.021 | .03577 |
| 21 | ↓ | ↓ | ↓ | .0152 | 8.197 | .03567 |
| 22 | ↓ | ↓ | ↓ | .0119 | 10.490 | .03434 |

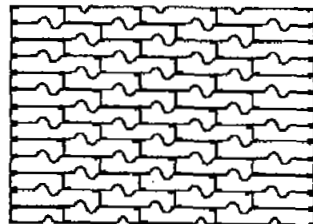


(a) Front view of segments 1 to 11.

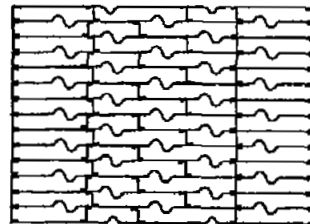
Figure 1. - Reactor mockup segments and assembly.



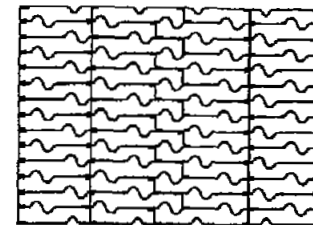
12



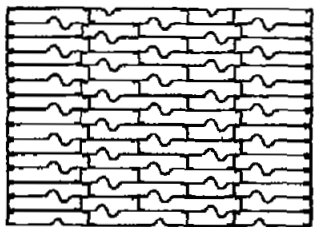
13



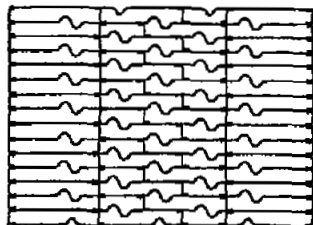
14



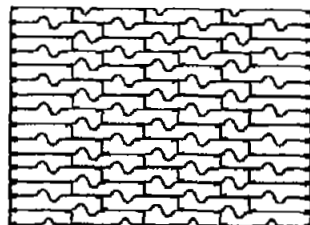
15



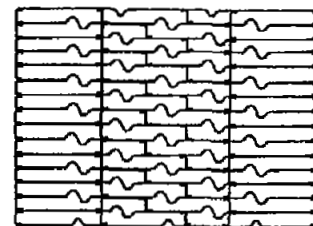
16



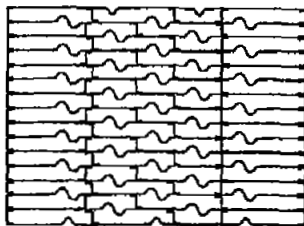
17



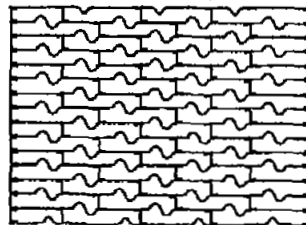
18



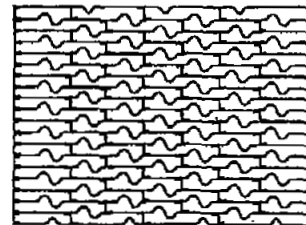
19



20



21

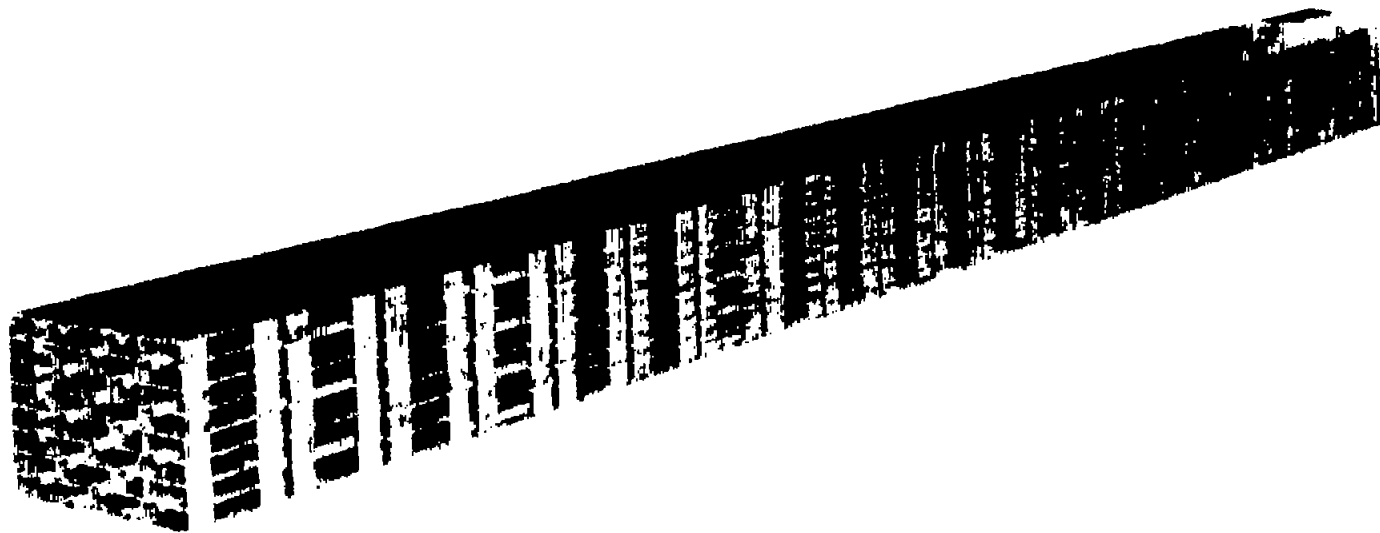


22

CD-4065

(b) Front view of segments 12 to 22.

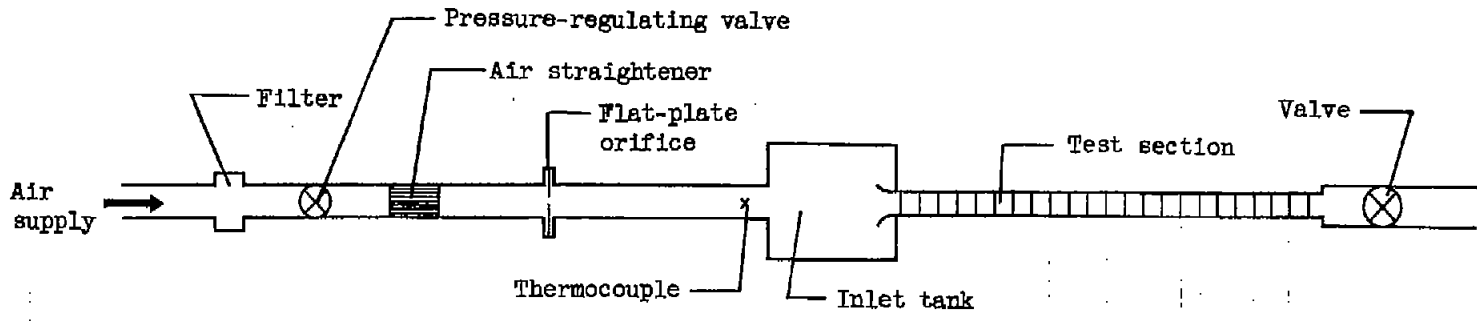
Figure 1. - Continued. Reactor mockup segments and assembly.



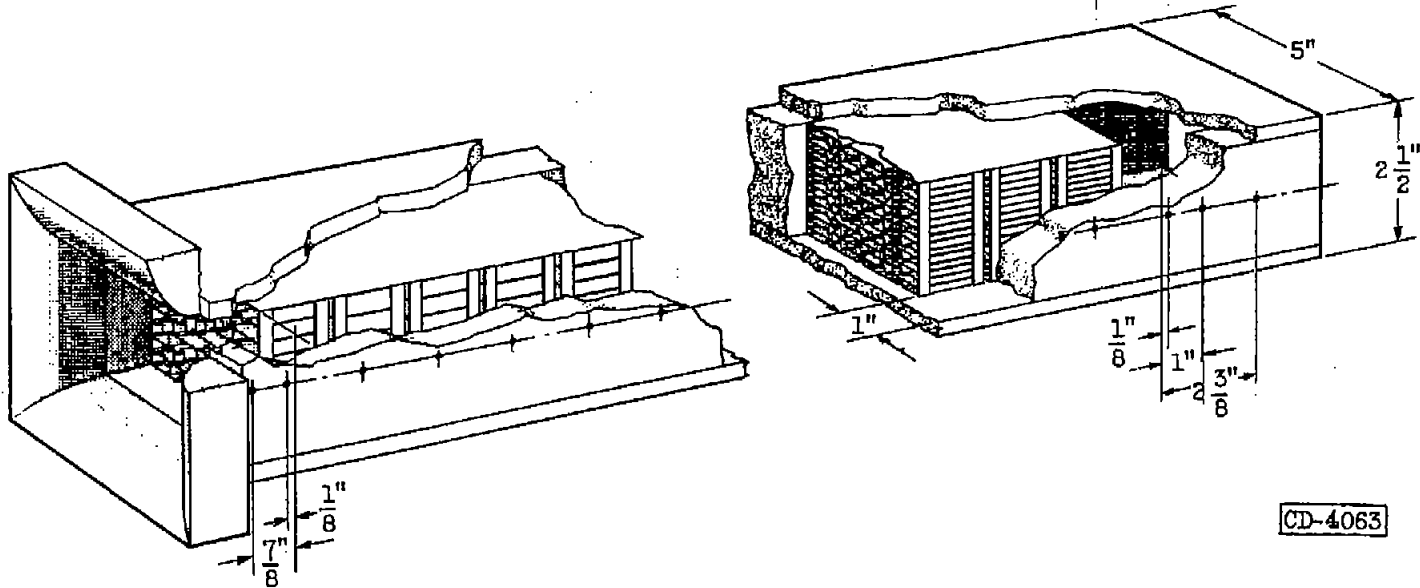
C-35155

(c) Assembled test section.

Figure 1. - Concluded. Reactor mockup segments and assembly.



(a) General layout.

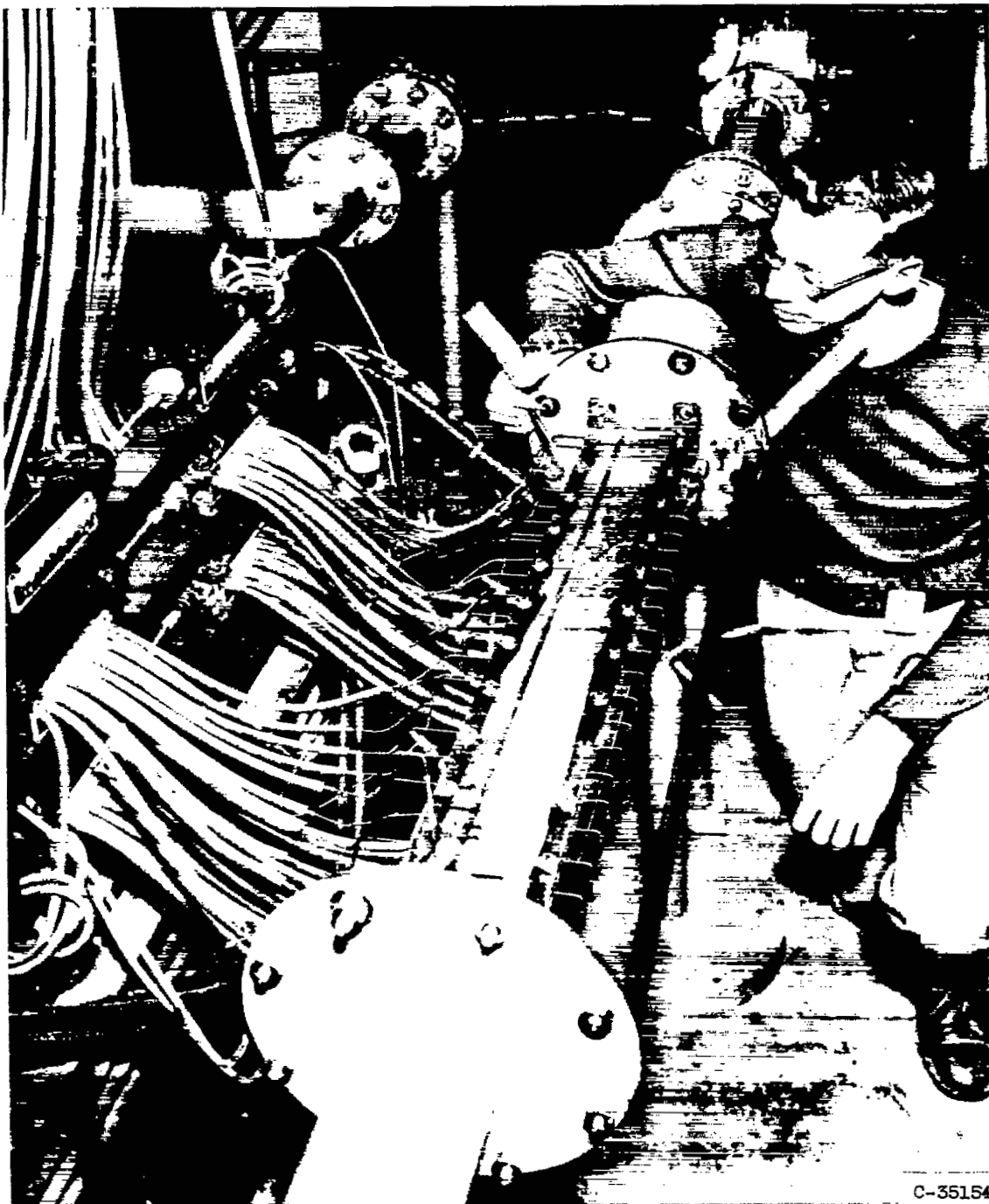


(b) Test section and metal tunnel.

Figure 2. - Schematic diagram of test setup.

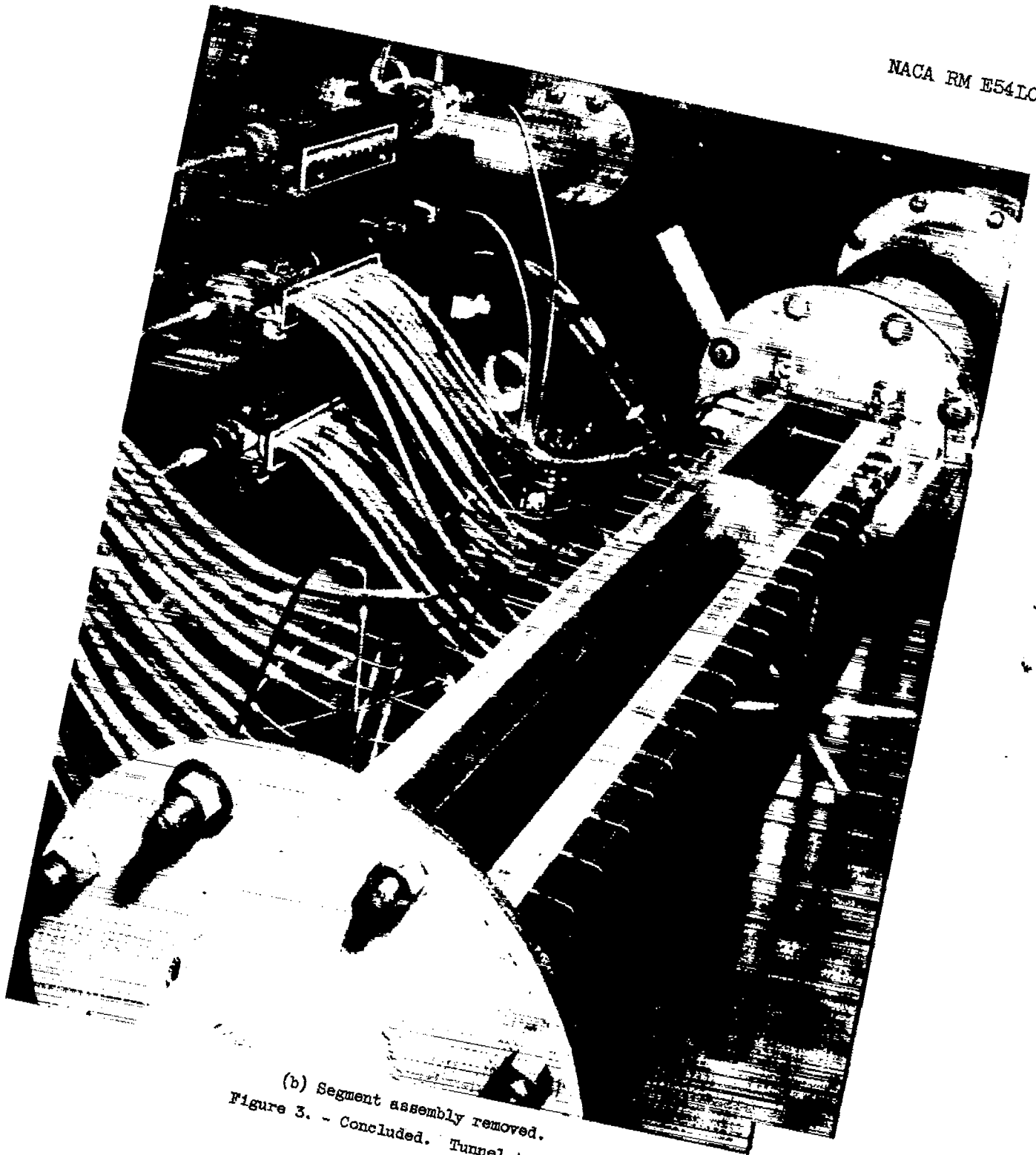
CD-4063

3504



C-35154

(a) Segment assembly enclosed.
Figure 3. - Tunnel test setup.



(b) Segment assembly removed.
Figure 3. - Concluded. Tunnel test setup.

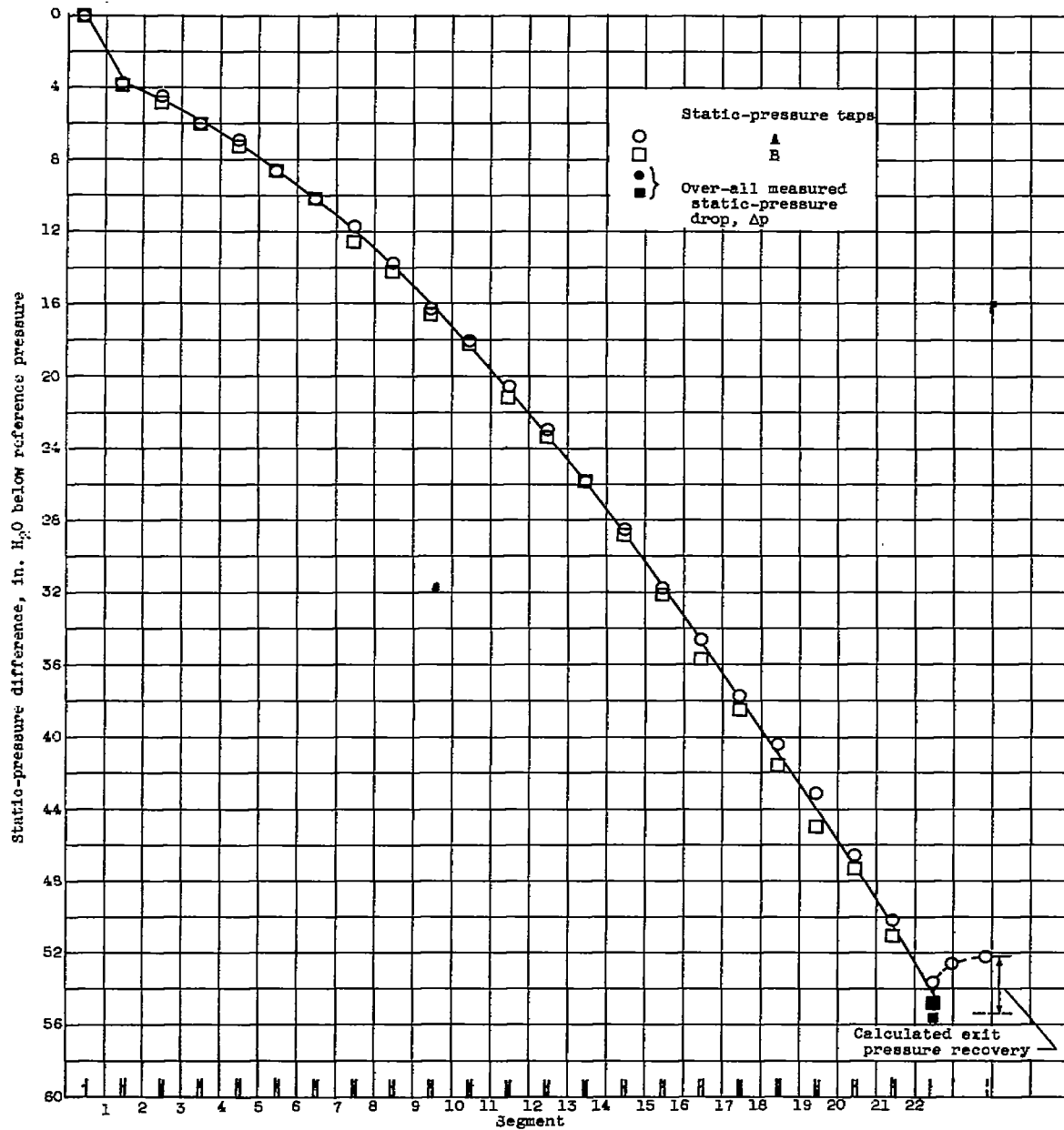
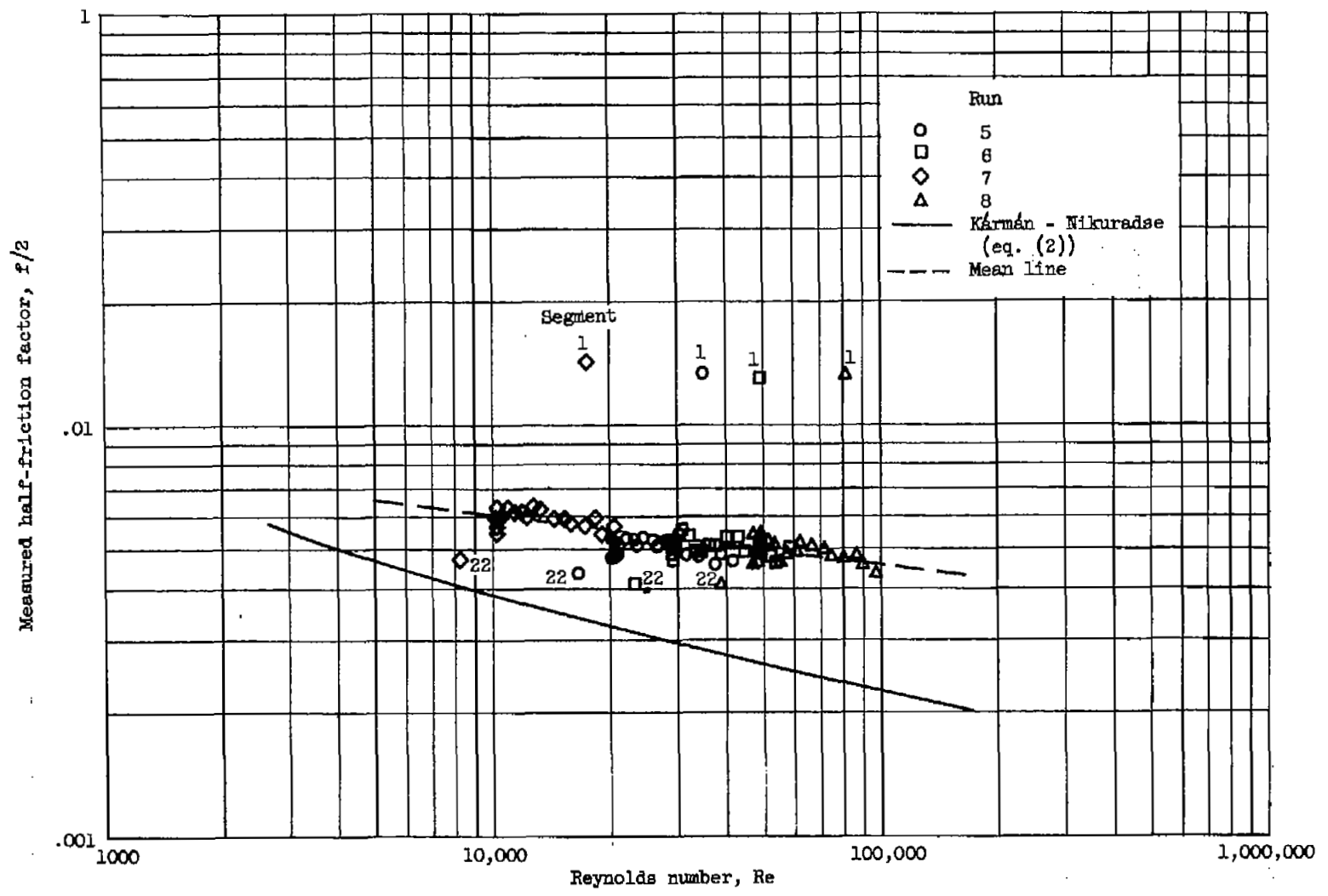
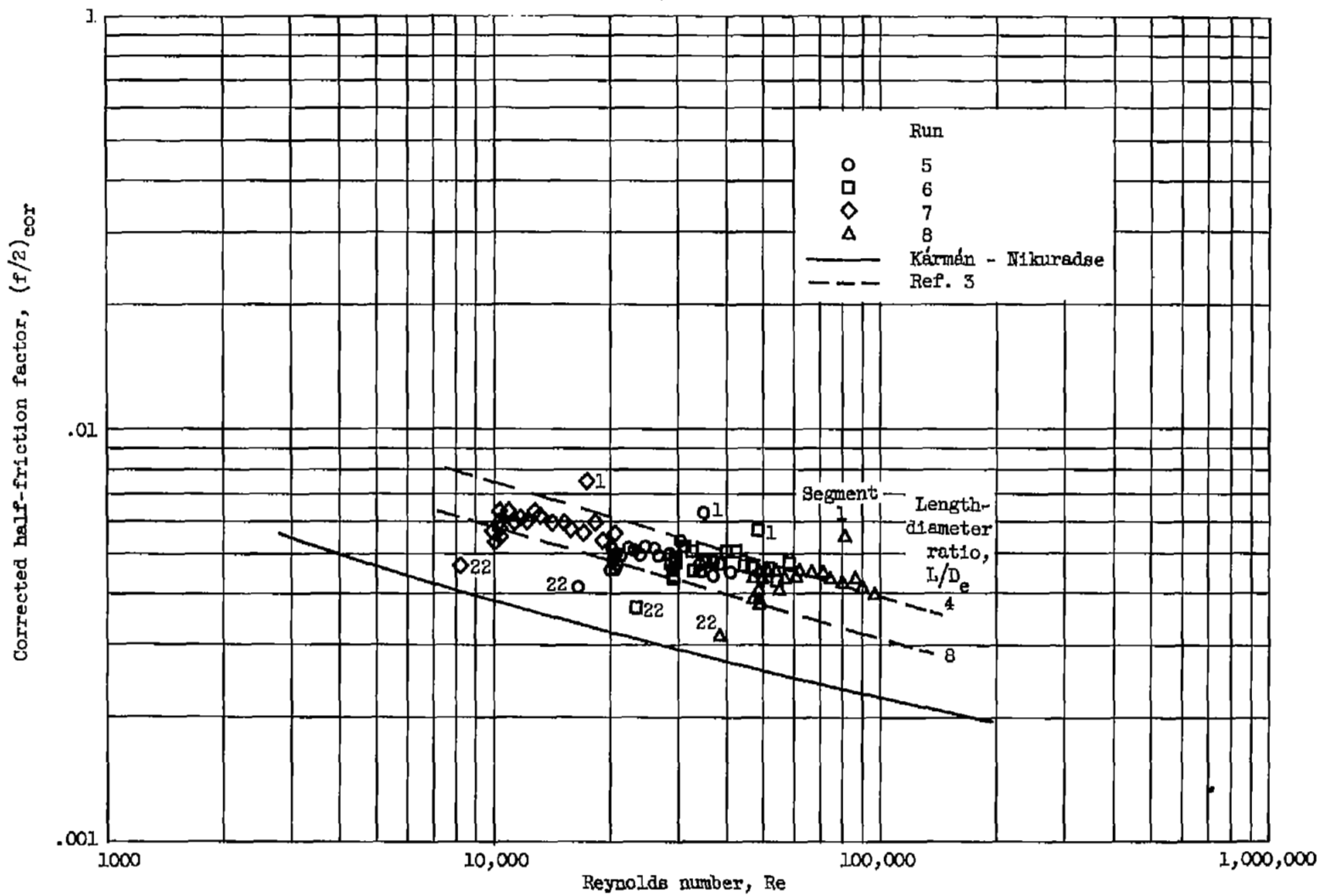


Figure 4. - Typical pressure-gradient curve for 22-segment assembly. Reference static pressure, 2378 pounds per square foot.



(a) Data based on measured static pressure drops (faired curve).
Figure 5. - Half-friction factors for reactor segments 1 to 22.



(b) Data based on measured pressure drops corrected for nonfriction losses.

Figure 5. - Concluded. Half-friction factors for reactor segments 1 to 22.

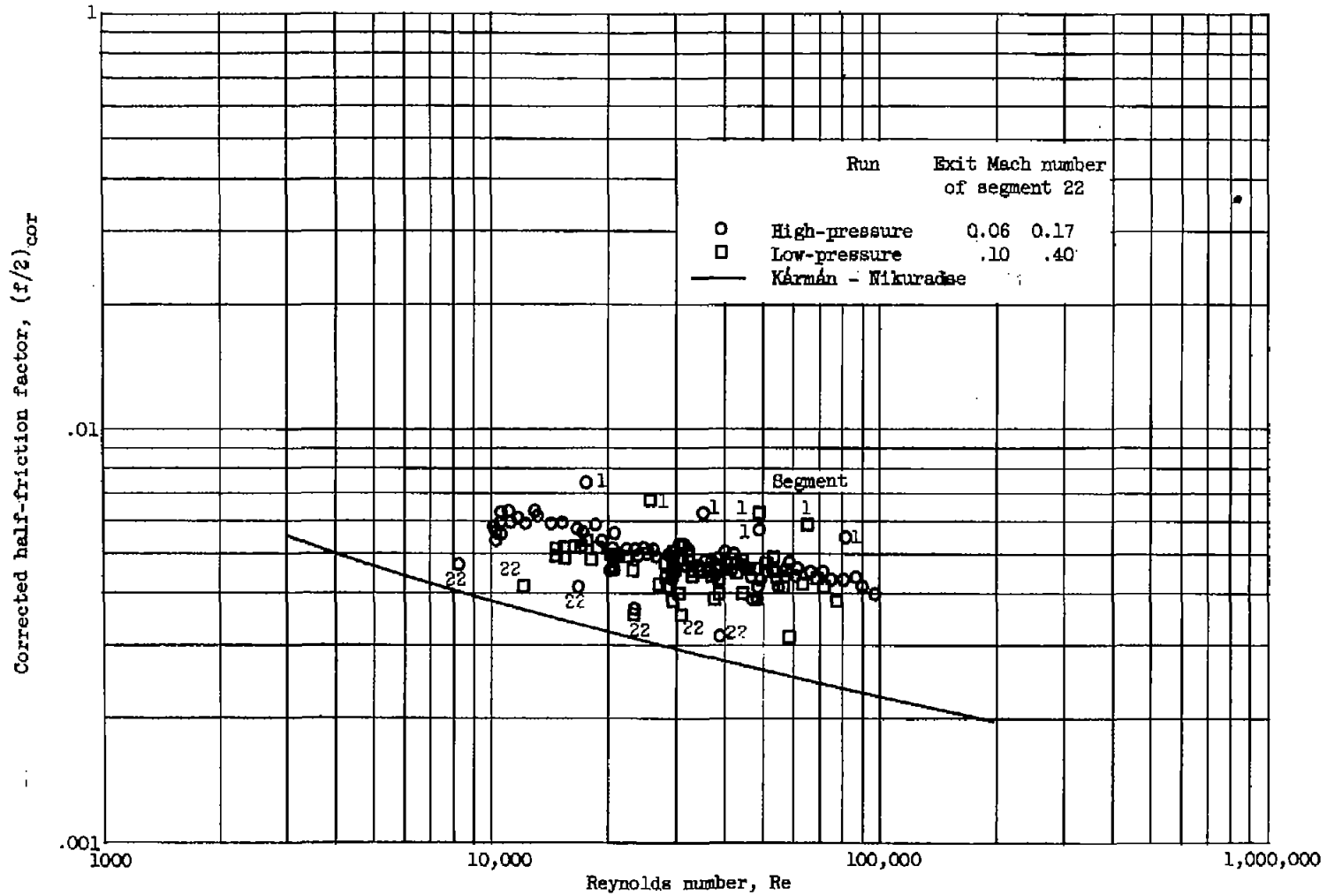


Figure 6. - Comparison of half-friction factors obtained at two pressure levels. Data based on measured pressure drops corrected for nonfriction losses.

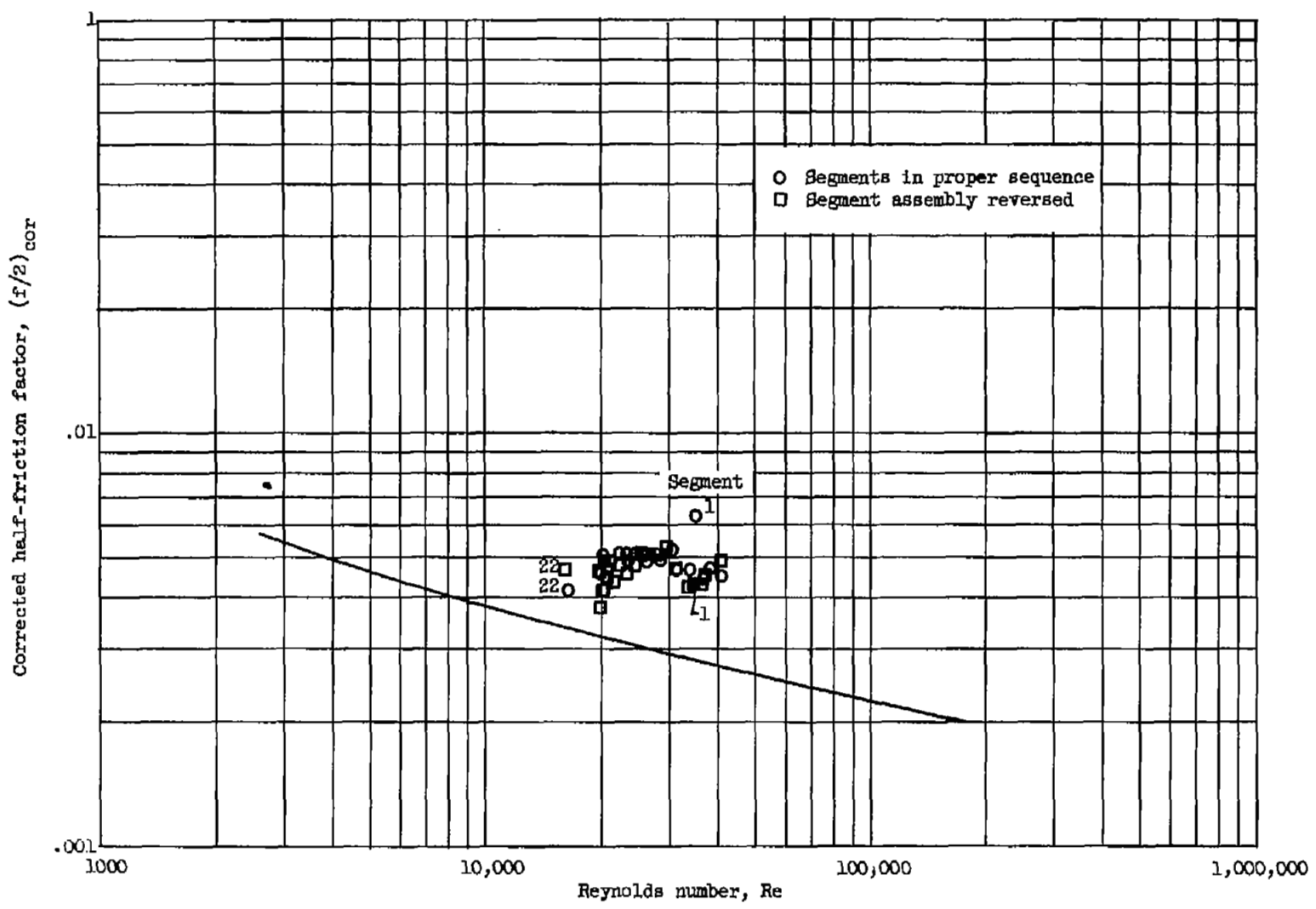


Figure 7. - Comparison of half-friction factors obtained with segments in proper sequence and with segment assembly reversed. Data for one flow rate based on measured pressure drops corrected for nonfriction losses.

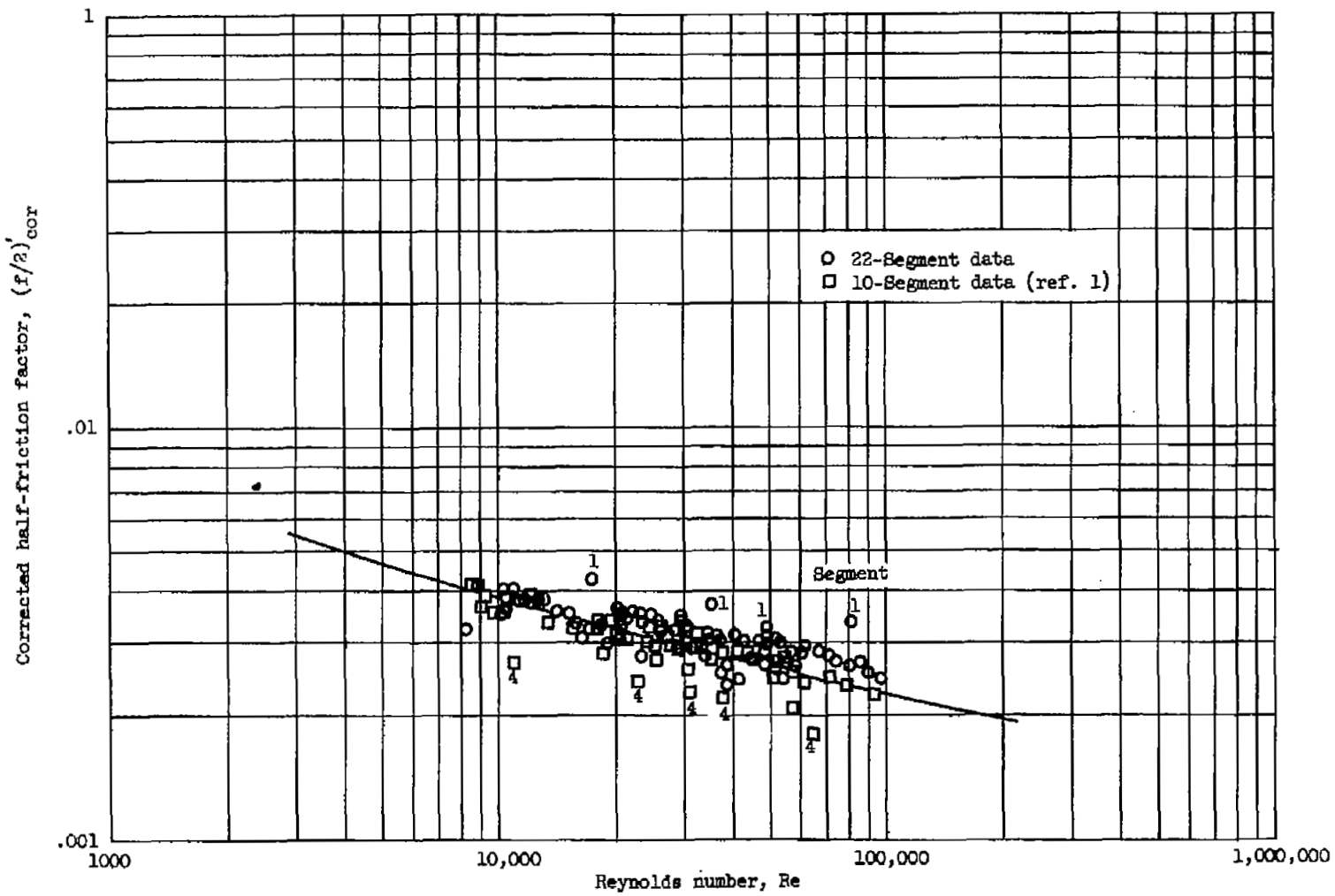


Figure 8. - Comparison of half-friction factors obtained herein with that of reference 1. Data based on measured pressure drops corrected for nonfriction losses and L/D_e effects.

NASA Technical Library



3 1176 01435 7744